Ab initio investigation of the screw dislocation-hydrogen interaction in bcc tungsten and iron

Pedro P.P.O. Borges, Emmanuel Clouet, Lisa Ventelon

Acta Materialia 234 (2022) 118048

Contents lists available at ScienceDirect

Acta Materialia

journal homepage: www.elsevier.com/locate/actamat

Ab initio investigation of the screw dislocation-hydrogen interaction in bcc tungsten and iron

Pedro P.P.O. Borges[1], Emmanuel Clouet[2], Lisa Ventelon*

Université Paris-Saclay, CEA, Service de Recherches de Métallurgie Physique, 91191, Gif-sur-Yvette, France

ARTICLE INFO

Article history:
Received 4 January 2022
Revised 12 May 2022
Accepted 18 May 2022
Available online 20 May 2022

Keywords:
Screw dislocations
Density functional theory
Tungsten
Iron
Hydrogen
Segregation

ABSTRACT

The interaction of hydrogen with $1/2 < 111 >$ screw dislocations is investigated in body-centered cubic tungsten and iron using *ab initio* calculations. Different core reconstructions are evidenced, depending on the number of hydrogen atoms introduced inside the dislocation core. Corresponding interaction energies are highly attractive in both metals, with a significant contribution of zero point energy associated with H vibrations, particularly in Fe. The pinning by hydrogen of the dislocation in its reconstructed core remains efficient for a local atomic fraction of hydrogen as low as 1/5. Other octahedral interstitial sites close to the reconstructed core are also attractive, contrary to the perfect bcc crystal where these sites are unstable and where hydrogen lies in the tetrahedral sites. Hydrogen recovers its bulk behavior only beyond the eighteenth neighbor octahedral sites. A simple pair interaction model is parameterized on *ab initio* calculations and used with a mean-field approximation to predict the concentration profiles of hydrogen segregated in and around the dislocation core. This segregation model predicts that dislocation core-sites remain completely decorated by hydrogen atoms up to at least 750 K and 200 K in W and Fe, respectively.

1. Introduction

The degradation of mechanical performance induced by hydrogen is a well-known phenomenon referred as hydrogen embrittlement, which can cause in-service deleterious fracture of structural components such as those used for hydrogen storage and in nuclear power plants. This complex material and environmental dependent process has been addressed through different experimental and modeling works in the past decades, providing insight into the deformation processes occurring in metals with the presence of hydrogen [1,2]. However, the mechanisms controlling hydrogen embrittlement remain uncertain. Among the different possible mechanisms, it is clear that hydrogen addition impacts the mobility of dislocations, in particular screw dislocations [3–5]. Thus, the investigation of the interaction between dislocations and hydrogen at the atomic scale may provide insightful knowledge of the mechanisms responsible for hydrogen embrittlement, and hence of the design of new safe structures resistant to embrittlement.

Plasticity of body centered cubic (bcc) metals, such as tungsten and iron, is dominated by screw dislocations with $1/2 < 111 >$ Burgers vectors [6,7]. Previous Density Functional Theory (DFT) works have predicted a strong interaction between the core of screw dislocations, *i.e.* the region in the immediate vicinity of dislocation lines, and both substitutional and interstitial solutes in bcc metals, which can lead to spontaneous reconstructions of the dislocation core towards configurations that are unstable in pure bcc metals [8–18]. More specifically in the case of hydrogen interstitial solutes, previous DFT studies in tungsten have shown an attractive interaction between the core of screw dislocations and hydrogen [19,20], with a spontaneous reconstruction of the dislocation core, from its easy core (*i.e.* the dislocation ground state in the pure metal) towards a split core, where the dislocation is centered in the immediate vicinity of a $\langle 111 \rangle$ atomic column [21]. In iron, strong binding sites for hydrogen corresponding to regions of low electron density around the dislocation core have been identified using DFT calculations [22]. Moreover, DFT calculations show that H atoms modify the Peierls energy barrier opposing glide of screw dislocations [21,23], thus impacting their mobility as simulated with kinetic Monte Carlo [24] or as seen experimentally *in situ* with transmission electron microscopy [3,5].

* Corresponding author
E-mail addresses: pedro_borges@berkeley.edu (P.P.P.O. Borges), lisa.ventelon@cea.fr (L. Ventelon).
[1] Present address: Department of Materials Science and Engineering, University of California, Berkeley, CA 94720, USA.
[2] Emmanuel Clouet was an associate Editor of the journal during the review period of the article. To avoid a conflict of interest, Emmanuel Clouet was blinded to the record and another editor processed this manuscript.

https://doi.org/10.1016/j.actamat.2022.118048
1359-6454/

This work proposes to investigate the interaction of hydrogen with the screw dislocation in both bcc tungsten and iron using DFT calculations. First, the hydrogen behavior in perfect bcc crystal is studied, focusing on the stability of the different insertion sites, on the diffusion and on the interaction between hydrogen atoms. Then, we model the effect of hydrogen on the core structure of screw dislocations, describing the different core reconstructions of the screw dislocation and the corresponding interaction energies for various numbers of hydrogen atoms in the core. We also examine other possible attractive sites for hydrogen around the reconstructed core. Finally, DFT results are used to parameterize an Ising energy model, which is combined with a mean-field approximation to predict hydrogen concentrations profiles in and around the dislocation core, giving a full picture of equilibrium segregation as a function of temperature.

2. Methodology

2.1. DFT calculations

DFT calculations are performed with the Vienna *Ab initio* Simulation Package (VASP) code [25–27]. We use pseudopotentials built with the projected-augmented-wave method [28,29] with a kinetic energy cutoff of 400 eV. Only 5d and 6s electrons for tungsten and 4s and 3d electrons for iron are included in valence states. Spin-polarized calculations are performed for iron. The exchange-correlation is described within the generalized gradient approximation with the Perdew-Burke-Ernzerhof functional [30]. Residual forces after ionic relaxation are inferior to 10^{-2} eV/Å. It is verified that a more rigorous force convergence criterion does not affect the results. All calculations are performed at constant cell volume and the Methfessel-Paxton scheme [31] to broaden the electronic density of states is employed with a smearing of 0.2 eV.

Energy barriers are determined using the climbing image nudged elastic band (cNEB) method [32,33]. cNEB calculations are performed using a spring constant of 5.0 eV/Å^2 and atomic positions are relaxed using the same criteria as for static calculations.

2.2. Zero point energy contribution

Zero point energy (ZPE) contribution is calculated from the Hessian matrix eigenvalues. We assume that metal atoms are heavy enough compared to hydrogen atoms to consider only the eigenvalues attributed to hydrogen. The Hessian matrix is computed by displacing each hydrogen atom in each direction by two small positive and negative displacements (±0.015 Å and ±0.030 Å). According to the harmonic approximation, the ZPE contribution is calculated as:

$$E_{ZPE} = \frac{1}{2}\sum_{i}^{3n} \hbar\sqrt{\frac{\lambda_i}{m_H}}, \tag{1}$$

where n is the number of hydrogen atoms in the system, λ_i are the eigenvalues of the $3n \times 3n$ Hessian matrix, m_H is the mass of a hydrogen atom and $\hbar$ is the reduced Planck's constant. The ZPE contribution for a H_2 molecule is 0.26 eV according to our calculations, which is in very good agreement with other DFT studies that also used the harmonic approximation [22,34,35].

2.3. Simulation cells

Calculations in perfect bulk are performed in a 5-unit cubic cell (250 atoms) using a $4 \times 4 \times 4$ shifted k-point grid to sample the Brillouin zone. Using the parameters presented in §2.1, the lattice parameter (a) is equal to 3.173 Å and 2.830 Å for tungsten and iron respectively, and the elastic constants are C_{11} = 497 GPa, C_{12} = 227 GPa and C_{44} = 131 GPa for tungsten, and C_{11} = 299 GPa, C_{12} = 153 GPa and C_{44} = 103 GPa for iron.

The dislocation calculations are performed using a periodic array of dislocation dipoles with a quadrupolar arrangement [36,37]. The cell vectors $\{\mathbf{p}_1, \mathbf{p}_2, \mathbf{p}_3\}$ are defined as: $\mathbf{p}_1 = 5/2\,\mathbf{u}_1 - 9/2\,\mathbf{u}_2$, $\mathbf{p}_2 = 5/2\,\mathbf{u}_1 + 9/2\,\mathbf{u}_2$ and $\mathbf{p}_3 = \mathbf{u}_3$, where the elementary vectors are $\mathbf{u}_1 = [-1\,-12]$, $\mathbf{u}_2 = [1\,-10]$ and $\mathbf{u}_3 = 1/2\,[111]$. Such configuration leads to a simulation cell containing 135 metal atoms per b along the $\langle 111\rangle$ direction (b is the norm of the dislocation Burgers vector, with $\vec{b} = a/2\,[111]$), with triperiodic boundary conditions. The separation distance between the dislocations of the dipole is equal to 15 $a\sqrt{6}/6$ in the $(1\bar{1}0)$ plane. This setup was proved to be large enough to provide well-converged energies [38,39]. We obtain an energy difference between the hard core configuration of the screw dislocation and its easy core ground state (ΔE_{H-E}) of 0.13 eV/b and 0.04 eV/b respectively in pure tungsten and iron, in good agreement with previous DFT works [14,18,40]. In order to study various hydrogen atomic fractions, the dislocation cell is then duplicated along the $\langle 111\rangle$ axis up to five times. For the 1b simulation cell described above, a $2 \times 2 \times 16$ shifted k-point grid is used to sample the Brillouin zone. The numbers of k-points used along the Z reciprocal direction are 8, 6, 4 and 4 for cell heights h = 2b, 3b, 4b and 5b, respectively.

An equal number of hydrogen atoms is inserted in the cores of both dislocations of the dipole at the same relative positions *i.e.*, according to the symmetry of the bcc lattice. We verify that in all our calculations, both dislocations and hydrogen atoms relax towards the same configuration. The screw dislocation-hydrogen interaction energy is defined by:

$$E_{int}^{n} = 1/2\,(E_{D+nH} - E_D) - n(E_{bulk+H} - E_{bulk}), \tag{2}$$

where n is the number of hydrogen atoms on each dislocation core. E_{D+nH} and E_D are the energies of the same cell containing both the dislocation dipole and hydrogen atoms, and only the dislocation dipole with the dislocations in their easy core ground state, respectively. E_{bulk+H} and E_{bulk} are the energies of the bulk cell respectively with and without a hydrogen atom in its stable tetrahedral position. With such a definition, a negative interaction energy implies attraction between the hydrogen atoms and the screw dislocation. When an increasing number of hydrogen atoms is inserted in the vicinity of the screw dislocation core, we define an incremental interaction energy (ΔE_{int}), which is expressed as:

$$\Delta E_{int} = E_{int}^{n} - E_{int}^{n-1}, \tag{3}$$

describing the interaction energy of the last arriving hydrogen atom in the already populated dislocation core.

3. Hydrogen in bulk

We first study the hydrogen behavior in bulk bcc W and Fe, focusing on the stability of the different interstitial sites and on hydrogen diffusion. We then investigate H-H pair interactions as a function of the separation distance between hydrogen atoms.

3.1. Dissolution and diffusion of hydrogen

The solution energy of a hydrogen atom in a tetrahedral (T) interstitial site is calculated using:

$$E_{sol} = E_{bulk+H} - E_{bulk} - 1/2\,E_{H_2}, \tag{4}$$

where E_{H_2} is the reference state energy of the H_2 molecule in vacuum (the 1/2 factor implies energy per atom). The hydrogen solution energies in tungsten and iron are respectively 0.93 (1.07) eV and 0.22 (0.33) eV (solution energies including ZPE contributions are given in parentheses). These values are in good agreement with those found by previous DFT studies in tungsten [41,42] and iron

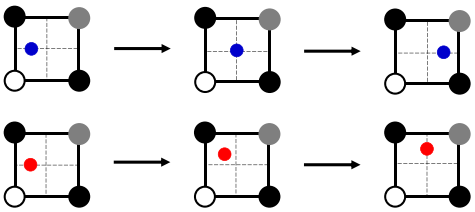

(a)

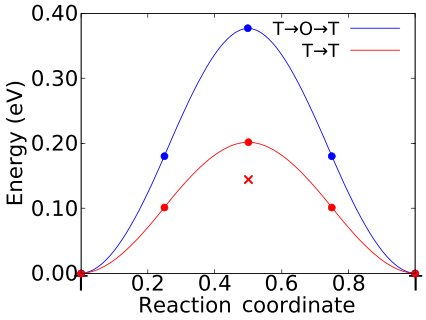

(b) W

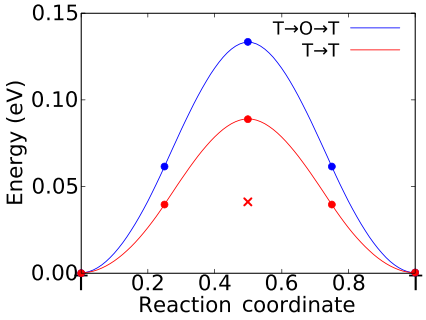

(c) Fe

Fig. 1. (a) Schematic representation (initial, saddle point and final configurations) of the two possible paths for hydrogen diffusion. Corresponding energy profiles in (b) bulk W and (c) bulk Fe: by crossing an O-site (in blue) and between two nearest neighbor T-sites (in red). The DFT calculations are represented by circles and the crosses indicate the T→T energy barrier in both metals after taking into account the ZPE contribution. (For interpretation of the references to color in this figure legend, the reader is referred to the web version of this article.)

[35,43,44]. We highlight the fact that ZPE contributions represent a significant part of the solution energies, especially in iron (∼ 30%). Taking into account ZPE contributions, these solution energies are in good agreement with the experimental values both in W and Fe (1.04 eV in W [45] and 0.30 eV in Fe [46,47]).

Hydrogen can diffuse between T-sites in the {100} plane through two possible paths: directly towards its nearest neighbor T-site (T→T) or by crossing an octahedral (O) site (T→O→T) in a ⟨100⟩ direction as shown in Fig. 1a. As shown in Fig. 1, the T→T path is energetically more favorable in both metals, in good agreement with previous DFT studies in tungsten [42,48] and iron [34]. We now take a closer look at the saddle point of both paths, calling attention to the normal modes of hydrogen. Table 1 gives the vibrational frequencies of the T-site and O-site as well as the T→T saddle point. In the case of the T-site, all normal mode frequencies are real, indicating that this configuration is stable and corresponds to the ground state. The O-site leads to two imaginary vibrational frequencies, with only the normal mode frequency perpendicular

Table 1
Diffusion barriers (ΔE) and vibrational frequencies (ν) of a hydrogen atom in a tetrahedral (T) site, octahedral (O) site and T→T saddle point in bulk W and Fe. The values including ZPE contributions are given in parentheses.

	Site	ΔE (eV)	ν (THz)
W	T	0	46, 46, 35
	O	0.38	74, *i*25, *i*25
	T→T	0.20 (0.14)	63, 45, *i*24
Fe	T	0	43, 43, 29
	O	0.13	64, *i*16, *i*16
	T→T	0.09 (0.04)	56, 36, *i*21

to the {100} plane being real. O-sites are thus unstable and, with more than one imaginary frequency, cannot even be considered as a saddle point between two T sites. The T→O→T transition path is artificially stabilized in the NEB calculations by the symmetries of the bcc network, which are preserved along the ⟨100⟩ diffusion direction, and does not correspond to a true migration path for hydrogen diffusion. On the other hand, the saddle point of the T→T path is a stationary point of rank one *i.e.*, with only one imaginary normal mode frequency, indicating that the T→T transition goes through a true saddle point. ZPE contributions to the energy barriers of this T→T transition (Table 1 and Fig. 1) are significant and lower the diffusion barriers, especially in the case of iron where it halves the diffusion barrier of hydrogen.

3.2. Hydrogen pair interaction

As obtained in the previous section, T-sites are the ground state for hydrogen in the bcc lattice. The hydrogen-hydrogen interaction energies are computed for various neighboring tetrahedral sites of one tetrahedral site, up to the maximum separation distance allowed by the simulation cell. Thus, within the bcc lattice, two hydrogen atoms are placed into two T-sites separated by various distances ranging from 0.35 a to 3.16 a. Fig. 2a shows a schematic representation of the ten first nearest neighbors of an initial hydrogen atom inserted in a tetrahedral site. The H-H pair interaction energy (V_{HH}) is calculated as:

$$V_{HH}(d_{HH}) = E_{bulk+2H} - 2 \times E_{bulk+H} + E_{bulk}, \quad (5)$$

where d_{HH} is the separation distance between the two hydrogen atoms, E_{bulk} is the energy of the pure metal bulk cell, E_{bulk+H} and $E_{bulk+2H}$ are the energies of the same cell with one and two hydrogen atoms, respectively. With such a definition, repulsion between the two hydrogen atoms leads to a positive interaction energy. Since ZPE contributions are computationally expensive, we chose to neglect them in the calculation of the H-H interaction energy. These calculations show that the H-H pair interaction is strongly repulsive at short distances ($d_{HH} < 0.7\ a$) and evidence a very weakly attractive interaction energy corresponding to a separation distance of 0.7 a in both metals (Fig. 2), in excellent agreement with previous DFT studies in tungsten [42,49]. Note that considering configuration 1 in Fig. 2a, the second hydrogen atom cannot be accommodated in this position in iron. In this case, ionic relaxation leads the second hydrogen atom towards a neighboring unit cell. According to these interaction energies, within a perfect metal crystal without any structural defect or surface/interface, the self-trapping of hydrogen is almost impossible due to the strongly repulsive energy between the two hydrogen atoms.

Analyzing larger separation distances between hydrogen atoms ($d_{HH} > a$), we observe an oscillatory behavior of the interaction energy. We attribute these energy fluctuations to the so-called Friedel oscillations, which arise from localized perturbations in the metallic electronic density caused by an impurity (hydrogen atoms) in

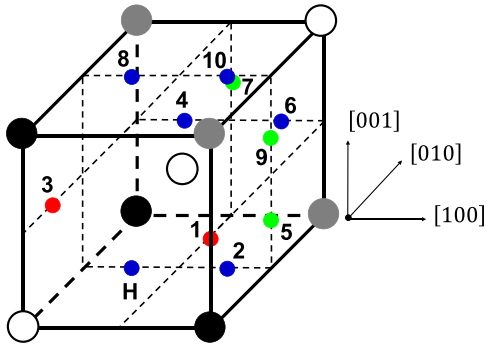

(a)

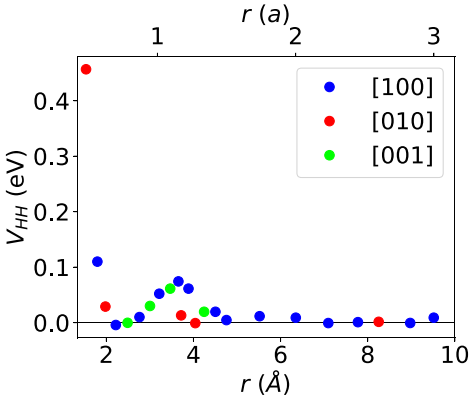

(b) W

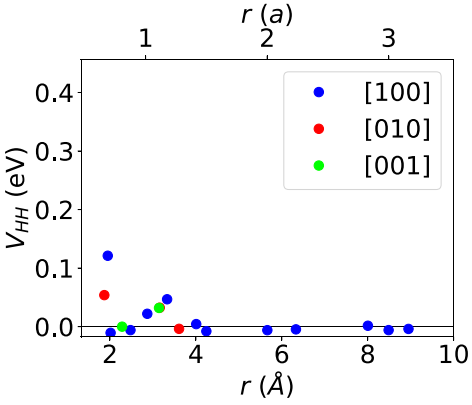

(c) Fe

Fig. 2. (a) Schematic representation of the ten first nearest neighbor sites (represented by colored circles) of a hydrogen atom sitting on a tetrahedral site of the bcc lattice (labelled "H"). Blue, red and green colors correspond to the different variants of the T-sites, which are equivalent by symmetry but possess three different orientations. Interaction energies in (b) W and (c) Fe as a function of the separation distance between the two hydrogen atoms. (For interpretation of the references to color in this figure legend, the reader is referred to the web version of this article.)

the Fermi gas. The Friedel oscillations are damped with increasing distance between hydrogen atoms and the H-H pair interaction is very close to zero at separation distances larger than 2 a. Elastic interaction between H atoms superimpose over this electronic interaction, with an amplitude depending on the relative orientation of the two T interstitial sites occupied by an H atom. Both electronic and elastic interaction contribute to the long-range repulsion between H atoms.

4. Hydrogen atoms in the screw dislocation core

The stability of the T-sites located inside the dislocation core is investigated in both metals for a separation distance between hydrogen atoms along the ⟨111⟩ direction of 1b. Then the evolution of the identified low energy states is studied for larger separation distances between hydrogen atoms, corresponding to lower local H concentrations.

4.1. Reconstruction of the dislocation core

All the calculations presented in this section are performed using the cell containing 135 metal atoms and each hydrogen atom inserted in each dislocation core represents a column of hydrogen atoms along the Burgers vector direction. For both tungsten and iron, we start with the dislocation in its ground state, *i.e.* the easy core, and we introduce a hydrogen atom in one of the three variants of the T-site inside the dislocation core (Fig. 3a). Upon ionic relaxation, different core reconstructions are obtained in tungsten and iron. In the case of tungsten, the dislocation core spontaneously reorganizes towards the split core configuration (Fig. 3b-left). The same core reconstruction was observed in Ref. [21]. The dislocation center is shifted towards an atomic column and the hydrogen atom moves in a newly created distorted pyramidal site inside the split core (Fig. 4a). In the case of iron, we also observe a spontaneous dislocation core reconstruction but towards the hard core configuration (Fig. 3b-right), similar to the reconstruction already evidenced in iron with the addition of B, C, N, and O interstitial solute elements [17]. The dislocation center is shifted towards the neighboring downward triangle defined by the [111] iron atomic columns and the hydrogen atom moves in a newly created prismatic interstitial site inside the hard core (Fig. 4b). Note that in both metals, the same dislocation core reconstruction is systematically obtained when introducing the hydrogen atom in one of the three different T-sites inside the dislocation core. Since both the hard and split core configurations are unstable in pure bcc metals [40], we assess that the presence of hydrogen stabilizes the split and the hard cores in tungsten and iron, respectively.

The screw dislocation-hydrogen interaction energies associated with these core reconstructions are strongly attractive in both metals (Table 2), in good agreement with another DFT study in Fe [22]. The calculated normal mode frequencies of hydrogen are all real (Table 2), indicating that the solute configuration is stable inside the reconstructed core. Corresponding ZPE contributions to the interaction energies reinforce the attraction between the screw dislocation and the hydrogen atom in both metals. Vibrational frequencies associated with the prismatic interstitial site in Fe are lower than in W, leading to a larger ZPE contribution in Fe.

Since relaxed configurations in tungsten and iron differ, we perform additional calculations considering different initial configurations. In the case of tungsten, the dislocation is initially relaxed in its hard core configuration and one hydrogen atom is then inserted in the prismatic site inside the hard core. This configuration is stable, however its energy is 0.12 eV (without ZPE) higher than the energy of the reconstructed core (*i.e.* the split core), indicating that this configuration is not energetically favorable. In the case of iron, we investigate the split core configuration with one hydrogen atom inside the split core. The split core configuration is generated from the hard core configuration following the methodology described in Ref. [40]. The hydrogen atom is then introduced in the previously mentioned distorted pyramidal site. This configuration is shown to be stable but presents a slightly higher energy of 0.02 eV (without ZPE) than the energy of the reconstructed core

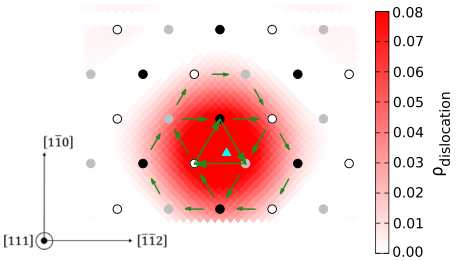

(a) Starting configuration

W **Fe**

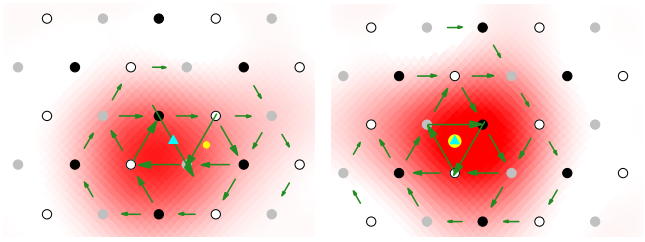

(b) One H atom per unit of *b*

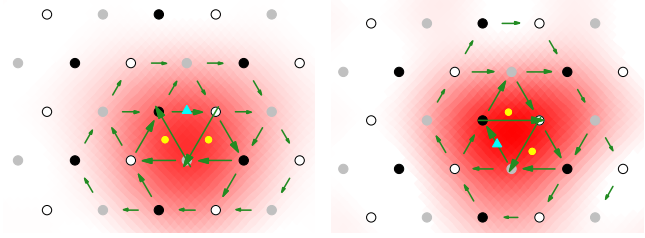

(c) Two H atoms per unit of *b*

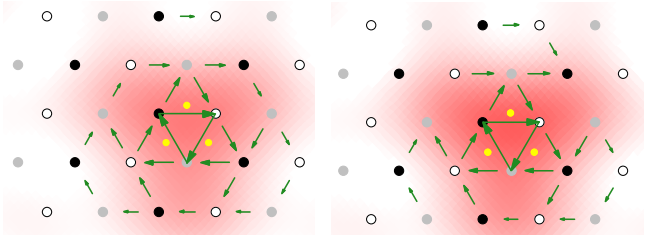

(d) Three H atoms per unit of *b*

Fig. 3. Dislocation core reconstruction with an increasing number of hydrogen atoms in the dislocation core. The atomic structure is projected in the (111) plane perpendicular to the dislocation line. Metal atoms are represented in white, gray and black, according to their original (111) plane in perfect bulk. The hydrogen atom is represented by a cyan triangle when it is introduced in the dislocation core before ionic relaxation and by a yellow circle after ionic relaxation. Arrows are drawn proportional to the relative displacements between [111] neighboring metal atomic columns along the Burgers vector direction and the contour map shows the dislocation density according to the Nye tensor, both corresponding to the relaxed configurations, except for structure (a), which corresponds to the starting configuration in both W and Fe (*i.e.* an easy core with one hydrogen atom in a T-site inside the dislocation core). Relaxed configurations in (b, c, d)-left correspond to W, while those in (b, c, d)-right correspond to Fe. (For interpretation of the references to color in this figure legend, the reader is referred to the web version of this article.)

(*i.e.* the hard core). In a nutshell, the configurations obtained in W and Fe following the spontaneous reorganization of the core structure are shown to be the low energy state for the screw dislocation core in the presence of one hydrogen atomic column in both metals. The different configurations obtained in tungsten and iron in the presence of one hydrogen atomic column, either the split core configuration or the hard core configuration, possibly arise

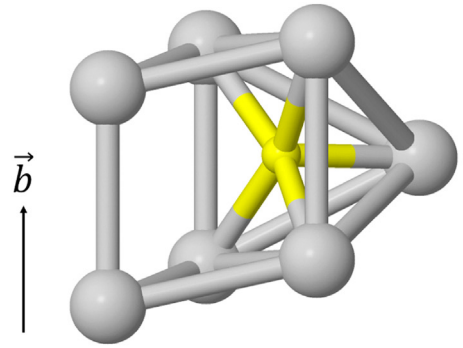

(a) W

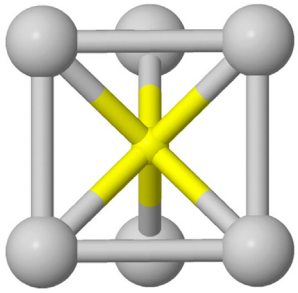

(b) Fe

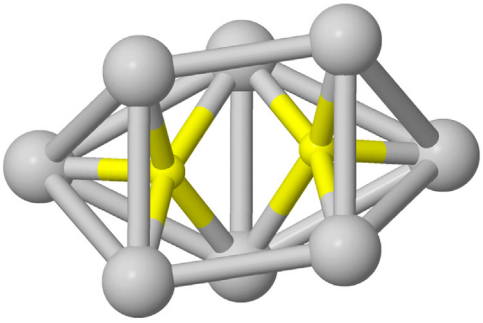

(c) W/Fe

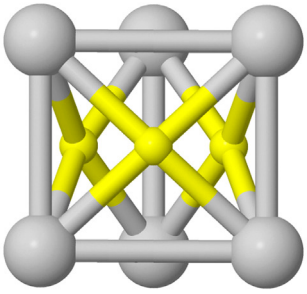

(d) W/Fe

Fig. 4. 3D visualization along the Burgers vector direction of the core structures corresponding to the low energy states of the screw dislocation in the presence of (a, b) one, (c) two and (d) three hydrogen atoms per unit of *b*. (a) Split core with one hydrogen atom in a distorted pyramidal site, (b) hard core with one hydrogen atom in the prismatic site in the center of the regular trigonal prism formed by the metal atoms, (c) split core with two distorted pyramidal sites decorated by hydrogen atoms and (d) hard core with three hydrogen atoms slightly shifted from the face centers of the trigonal prism. Configuration (a) corresponds to W, (b) to Fe, while (c) and (d) to both metals.

Table 2
Interaction of a screw dislocation with various numbers of H atoms in its core: core structures obtained upon ionic relaxation, total (E_{int}) and incremental (ΔE_{int}) interaction energies (Eqs. (2) and (3) respectively), and vibrational frequencies (ν) of the last introduced hydrogen atom. For interaction energies, the values including ZPE contributions are given in parentheses.

	H at./b	Core struct.	E_{int} (eV)	ΔE_{int} (eV)	ν (THz)
W	1	Split	−0.57 (−0.66)	-	34, 34, 26
	2	Split	−1.21 (−1.37)	−0.63 (−0.72)	35, 35, 30
	3	Hard	−1.87 (−2.09)	−0.63 (−0.72)	36, 36, 36
	4	Hard	−1.94 (−2.20)	−0.07 (−0.11)	26, 18, 18
Fe	1	Hard	−0.23 (−0.34)	-	22, 22, 20
	2	Split	−0.31 (−0.41)	−0.08 (−0.07)	36, 36, 32
	3	Hard	−0.39 (−0.56)	−0.08 (−0.15)	38, 38, 38
	4	Hard	+0.40 (+0.16)	+0.79 (+0.72)	21, 13, 13

from the different energy landscapes seen by the screw dislocation in pure metals. Notably, the hard core in iron is close to the saddle point of the dislocation Peierls barrier, with an energy cost only half than the one of the split core [40]. On the other hand, this hard core configuration is highly unstable in tungsten, where it corresponds to a strong maximum of the dislocation 2D energy landscape [40].

We then investigate the possibility to accommodate a second hydrogen atom inside the reconstructed dislocation core. We start with the previously obtained reconstructed cores, which are already decorated by one hydrogen atom per b in both metals. As illustrated in Fig. 3b, a second hydrogen atom is inserted in the neighboring empty pyramidal site in the case of tungsten and inside the prism formed by the metal atoms in the case of iron (at the same altitude than the metal atoms, *i.e.* separated by $b/2$ along the $\langle 111 \rangle$ direction from the first H atom). Upon ionic relaxation, we obtain the same core configuration in both metals: the split core configuration with each hydrogen atom located in a distorted pyramidal site (Figs. 3c and 4 c).

We further investigate the possibility to accommodate a third hydrogen atom inside the dislocation core. The additional hydrogen atom is inserted in the remaining empty pyramidal site of the split core configuration (Fig. 3c). Upon ionic relaxation, we observe a spontaneous dislocation core reconstruction towards the hard core configuration in both metals. The dislocation center is shifted towards the center of the downward triangle defined by the [111] metal atomic columns and the hydrogen atoms are slightly shifted from the face centers of the regular trigonal prism formed by the metal atoms (Figs. 4d and 3 d). The total interaction energies corresponding to the addition of this second and third H atom are attractive in both metals, with a non negligible contribution of ZPE (Table 2), especially in iron for the insertion of the third H atom. All incremental interaction energies are attractive, indicating that the addition of a second or of a third H atom on an already decorated dislocation is always favorable.

Lastly, we investigate the possibility to accommodate a fourth hydrogen atom inside the reconstructed dislocation core. Considering the dislocation in its hard core configuration with three hydrogen atoms located in the face centers of the prism, a fourth hydrogen atom is introduced in the prism center, at the same altitude than the other three hydrogen atoms (*i.e.* at $b/2$ if 0 stands for the altitude of the metal atoms). In both W and Fe, upon atomic relaxation, the hard core decorated by the three hydrogen atoms is stable while the fourth hydrogen atom relaxes along the $\langle 111 \rangle$ direction towards the center of the triangle formed by the three metal atoms, *i.e.* from $z = b/2$ to 0. This configuration is associated with a strongly repulsive incremental interaction energy of +0.79 eV in iron (+0.72 eV with ZPE) and a weakly attractive one of −0.07 eV in tungsten (−0.11 eV with ZPE).

Finally, once the low energy states of the screw dislocation are identified with an increasing number of hydrogen atoms inside the core, we investigate the evolution of the reconstructed dislocation cores with a decreasing number of hydrogen atoms. Starting with a fully populated core, one hydrogen atom is removed at a time, performing ionic relaxation at each step. In the case of tungsten, the configurations obtained with an increasing or a decreasing number of hydrogen atoms are identical. In iron, the decreasing process leads to a different configuration only in the case of a single hydrogen atom in the dislocation core, where we obtain the same split core configuration as in tungsten. As already discussed, this configuration has a higher energy in iron than the ground state obtained when increasing progressively the number of H atoms (difference of 0.02 eV without ZPE).

4.2. Dilute regime

We expand this study to larger separation distances between hydrogen atoms along the Burgers vector direction, *i.e.* using supercells of height greater than 1b. The interaction between the screw dislocation and hydrogen inside the core corresponds to a more complex situation than in the case of other interstitial solutes like B, C, N or O [14,16–18,50], since it involves the atomic fraction of hydrogen not only along the $\langle 111 \rangle$ axis but also in the (111) plane (up to three hydrogen atoms per unit of b can be accommodated inside the dislocation core). Here we consider a fully decorated dislocation core in the hard core position with three hydrogen atoms in a 1b-thick layer, and we then vary the hydrogen atomic fraction along the dislocation line. We investigate the evolution of the core structure for cells of height $h = 2b$, $3b$, $4b$ and $5b$ in both metals. It is found that in Fe, the trigonal prisms formed by the metal atoms in the hard core configuration remain regular with increasing H-H distance along b (Fig. 5b), while they become distorted in W (Fig. 5a).

To be more quantitative, we define a dislocation pinning coefficient, which takes form as:

$$\zeta = \frac{d_D}{d_{EH}}, \tag{6}$$

where d_{EH} is the distance between the easy and the hard core positions in the (111) plane and d_D is the distance between the easy core position and the dislocation position calculated in a given layer. Both d_{EH} and d_D are calculated along the $[1\bar{1}0]$ direction (see Fig. 5c). With such a definition, $\zeta = 0$, 1 and 2 indicates the easy, hard and split core positions, respectively. The dislocation position is calculated by fitting the differential displacements of $\langle 111 \rangle$ neighboring atomic columns along the Burgers vector direction extracted from our DFT calculations to the differential displacements predicted by linear elasticity theory solution [39]. The values for the pinning coefficient obtained layer-by-layer are presented in Table 3. In the case of tungsten, the dislocation core evolves towards a configuration in-between the hard and split cores, with a decreasing atomic fraction of hydrogen along the dislocation line. In the case of iron, the dislocation remains strongly pinned in the hard core configuration up to 5b. The difference between both metals arises from their different energy landscapes seen by the screw dislocation in pure W and Fe [40], as mentioned previously. Particularly, in contrast with tungsten, the hard core in iron has a

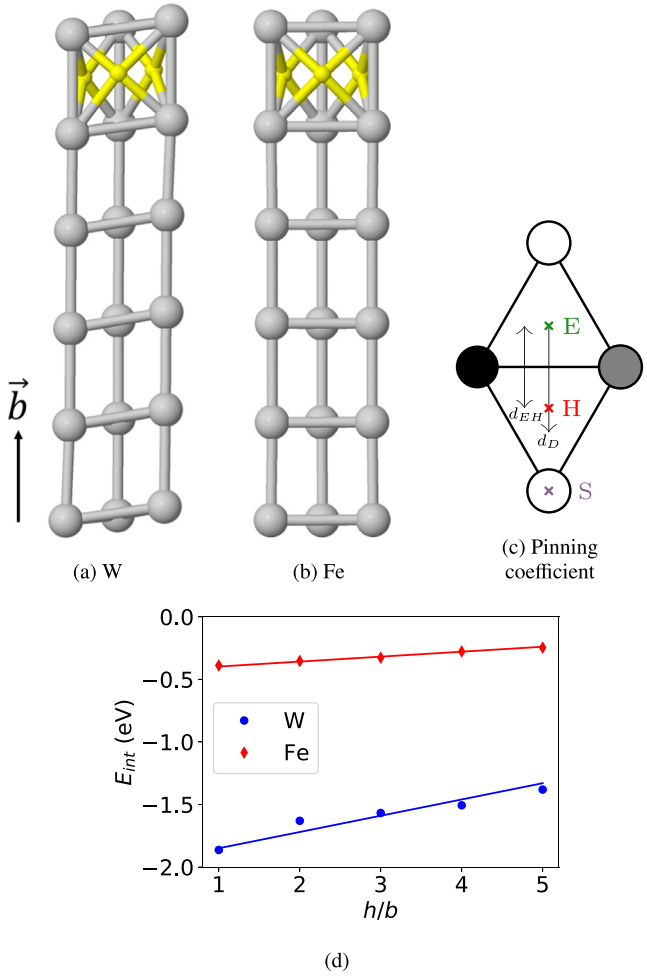

Fig. 5. 3D visualization along the Burgers vector direction of the core structures corresponding to a separation distance of 5*b* between fully saturated 1*b*-thick layers by hydrogen atoms in (a) W and (b) Fe. (c) Schematic definition of the dislocation pinning coefficient (Eq. (6)). (d) Total screw dislocation-hydrogen interaction energy (Eq. (2)) as a function of cell height. Scattered blue circles and red diamonds denote DFT calculations for tungsten and iron, respectively. Lines of respective colors indicate the interaction energies predicted by the model (Eq. (7)).

Table 3
Total screw dislocation-hydrogen interaction energy (E_{int}) and dislocation pinning coefficient as a function of cell height (h). Interaction energies do not include ZPE contributions and the dislocation pinning coefficient (ζ_i) is calculated in the i-layer of the cell.

	h	E_{int} (eV)	ζ_1	ζ_2	ζ_3	ζ_4	ζ_5
W	1*b*	−1.87	1.01	-	-	-	-
	2*b*	−1.63	1.33	1.32	-	-	-
	3*b*	−1.57	1.42	1.47	1.45	-	-
	4*b*	−1.51	1.49	1.55	1.56	1.52	-
	5*b*	−1.38	1.51	1.58	1.58	1.60	1.54
Fe	1*b*	−0.39	0.97	-	-	-	-
	2*b*	−0.35	0.99	0.97	-	-	-
	3*b*	−0.33	0.99	0.97	0.98	-	-
	4*b*	−0.28	1.06	1.08	1.09	1.08	-
	5*b*	−0.26	0.97	0.98	0.99	0.99	0.99

remarkably low energy compared to the split core, and thus the dislocation pinning in the hard core position induced by hydrogen segregation is energetically more favorable in iron than in tungsten.

We now examine the evolution of the screw dislocation-hydrogen interaction energy as a function of cell height. Table 3 presents the total interaction energies obtained from Eq. (2). ZPE contributions are not included in these calculations. A strong binding between the screw dislocation and the hydrogen atoms up to 5*b* is evidenced in both metals. If we neglect all pair interactions between hydrogen atoms in core-sites, namely the interaction between hydrogen atoms sitting on two core-sites belonging to two different (111) planes, the interaction energy can be expressed as:

$$E_{int}(h) = E_{int}^{(0)} + h\Delta E_{E-H}, \tag{7}$$

where h is the supercell height, $E_{int}^{(0)}$ is the interaction energy between the three hydrogen atoms and the hard core and ΔE_{E-H} is the energetic cost of transformation from an easy to a hard core per unit of length [14,16]. Fitting with the least-squares method, we obtain $E_{int}^{(0)} = -1.98$ eV for tungsten and $E_{int}^{(0)} = -0.44$ eV for iron. Figure 5d represents the interaction energies calculated using DFT and predicted using Eq. (7). The model provides an excellent prediction of the interaction energy in iron, thus showing that the interaction of hydrogen atoms in core-sites which are in different (111) planes can be safely neglected. In the case of tungsten, we observe that the model does not reproduce the DFT data as good as in iron, although it is still satisfactory. Small deviations observed between DFT data and the predicted interaction energies arise from the fact that the model of Eq. (7) considers a constant energetic cost to transform a dislocation segment from an easy to a hard core, while as shown in Table 3, the dislocation position extracted from our DFT calculations does not correspond exactly to the hard core and evolves towards a position in-between the hard and split cores with increasing separation distance between hydrogen atoms along *b*. In this way, as the cell height increases, the energetic cost of transformation from an easy to a reconstructed core is not strictly equal to $h\Delta E_{E-H}$ as considered in Eq. (7), leading to more pronounced differences in tungsten between the interaction energies predicted using the linear model and calculated with DFT.

5. Hydrogen segregation on dislocation cores

Once the most attractive sites for hydrogen in the dislocation core are identified, we investigate other interstitial sites around the reconstructed core, which are likely to attract hydrogen. Using DFT calculations, we calculate the interaction energies for these sites and the relevant interactions between hydrogen atoms. Based on these DFT data, we parameterize an Ising model and perform mean-field calculations in order to describe the hydrogen equilibrium segregation in these different sites inside and around the dislocation core.

5.1. Interstitial sites around the reconstructed core

As demonstrated in §3.1, T-sites are the ground state of hydrogen in the perfect bcc lattice. We start with a cell of height 1*b*, with the dislocation in the reconstructed hard core configuration and with all the three core-sites decorated by hydrogen atoms. Then, an additional hydrogen atom is inserted in a T-site around the reconstructed core. We investigate thirty-nine different T-sites which are 0.65 *a* up to 2.40 *a* distant (in the (111) plane) from the reconstructed dislocation core. Given the symmetry of the bcc network, this covers all existent T-sites around the reconstructed core (see Fig. 6). In each case, we compute the incremental screw dislocation-hydrogen interaction energy of the last arriving hydrogen atom (Eq. (3)).

As shown in Fig. 6, in most cases and for both W and Fe, when the additional hydrogen atom is inserted in a T-site, it relaxes towards a neighboring O-site leading to an attractive incremental interaction energy. The identified attractive O-sites correspond to

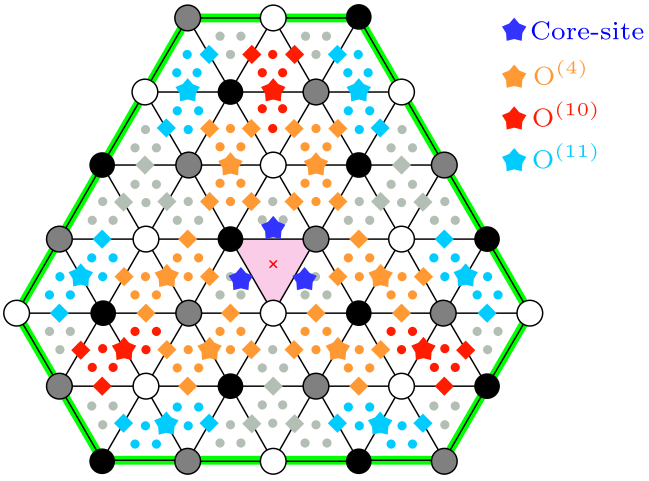

Fig. 6. Schematic representation of the investigated interstitial sites around the reconstructed core (represented by a light red triangle) projected in the (111) plane. Small gray circles represent T-sites, for which the additional hydrogen atom remains in its initial T-site, but leads to a repulsive incremental interaction energy between this T-site and the decorated dislocation core. Colored small circles denote T-sites, for which upon ionic relaxation, the hydrogen atom moves from its initial T-site towards an O-site, represented by stars of respective color. Diamonds indicate O-sites that are unstable for hydrogen: the solute either relaxes towards an attractive O-site (stars of respective color) or towards a repulsive T-site (small gray circles). The eighteenth neighbor octahedral sites of the reconstructed core are located on the green line. (For interpretation of the references to color in this figure legend, the reader is referred to the web version of this article.)

Table 4
Incremental screw dislocation-hydrogen interaction energy (ΔE_{int}) and vibrational frequencies (ν) of the identified attractive O-sites around the reconstructed core. The values including ZPE contributions are given in parentheses.

		ΔE_{int} (eV)	ν (THz)
W	$O^{(4)}$	−0.41 (−0.51)	27, 26, 26
	$O^{(10)}$	−0.26 (−0.34)	29, 28, 28
	$O^{(11)}$	−0.11 (−0.21)	27, 26, 26
Fe	$O^{(4)}$	−0.14 (−0.21)	23, 22, 22
	$O^{(10)}$	−0.08 (−0.17)	27, 26, 26
	$O^{(11)}$	−0.04 (−0.11)	24, 23, 23

the fourth, tenth and eleventh neighbors of the reconstructed dislocation core, denoted $O^{(4)}$, $O^{(10)}$ and $O^{(11)}$, respectively. The corresponding incremental interaction energies for those O-sites are given in Table 4. Meanwhile, for some T-sites, the additional hydrogen atom remains in its initial T-site, leading to a repulsive incremental interaction energy (see Fig. 6). We also verify that all other O-sites around the reconstructed core are unstable. Indeed, the hydrogen atom located in one of these sites either relaxes towards an attractive $O^{(4)}$, $O^{(10)}$ or $O^{(11)}$ site or towards a repulsive T-site. Beyond the eighteenth neighbor octahedral sites of the reconstructed core, which correspond to a distance of 2.40 a from the core in the (111) plane, hydrogen recovers its behavior in perfect bulk, *i.e.* it is stable in a T-site and its interaction energy with the decorated screw dislocation is very close to zero. $O^{(18)}$ sites and all the O-sites further from the core are unstable and the additional hydrogen atom introduced in one of these sites systematically moves towards a T-site.

Calculation of hydrogen vibration normal modes leads to real frequencies for the three $O^{(4)}$, $O^{(10)}$ and $O^{(11)}$ octahedral sites, both in iron and tungsten (Table 4). These octahedral sites near the reconstructed core are thus stable, in stark contrast with the perfect bcc crystal where octahedral sites are unstable. The ZPE contribution deduced from these frequencies increases the stability of $O^{(4)}$, $O^{(10)}$ and $O^{(11)}$ sites, leading to an incremental interaction energy which is more negative than the one without ZPE (Table 4). ZPE contributions associated with the studied O-sites are almost the same for the three stable octahedral sites, since normal modes for the different O-sites are close to each other. We note in particular that hydrogen vibration frequencies are high, even for the $O^{(11)}$ site, which is far from the reconstructed core.

5.2. Hydrogen segregation on dislocation cores

We now model the segregation of hydrogen on the screw dislocation. We consider the three core-sites corresponding to the face centers of the prisms defined by the hard core and the three octahedral sites, which have been found attractive around the reconstructed core. We neglect the fourth insertion site inside the core as this site has been found repulsive in iron and only weakly attractive in tungsten.

5.2.1. Ising Hamiltonian model

Based on the DFT results provided in section §5.1, we develop an Ising Hamiltonian [18,50] taking into account the core-sites and the identified attractive O-sites, which takes form as:

$$H = \sum_i \Delta E_i^{seg,0} p_i + \frac{1}{2} \sum_{i,j \neq i} V_{ij} p_i p_j + h \Delta E_{H-E}, \tag{8}$$

where $\Delta E_i^{seg,0}$ is the segregation energy on site i (with $i \in$ {core, $O^{(4)}$, $O^{(10)}$, $O^{(11)}$}) in the dilute limit and V_{ij} is the pair interaction between hydrogen atoms located on sites i and j. The site occupancy p_i is equal to 1 when site i is occupied by a hydrogen atom and to 0 otherwise. The last term, $h\Delta E_{H-E}$, corresponds to the energy cost of transformation of a dislocation segment of length h from an easy to a hard core. The inclusion of this term arises from the fact that the easy core is considered as the reference state in the calculation of the screw dislocation-hydrogen interaction energy (Eq. (2)). Such an Ising model is fully equivalent to a cluster expansion [51] with effective interactions depending on sites relative positions to the dislocation core, as already developed, for instance, in Mo-W bcc solid solutions containing dislocations [52].

To fit the parameters of the Hamiltonian, we perform DFT calculations using cells of height 1b and 2b. We assume that hydrogen atoms do not interact when their separation distance is larger than 2b along the Burgers vector direction, in agreement with the behavior observed for the core-sites (*cf.* §4.2). Four different pair interactions are included in Eq. (8) as it is proved to be sufficient to describe the interaction between hydrogen atoms. We take into account the pair interaction between $O^{(4)}$ sites that are close neighbors in the (111) plane ($V_{12}^{O^{(4)}}$) and in different (111) planes ($V_{12'}^{O^{(4)}}$), as illustrated in Fig. 7b. Note that by symmetry $V_{12}^{O^{(4)}} = V_{34}^{O^{(4)}} = V_{56}^{O^{(4)}}$ and $V_{12'}^{O^{(4)}} = V_{34'}^{O^{(4)}} = V_{56'}^{O^{(4)}}$. We also consider the pair interaction between $O^{(10)}$ and $O^{(11)}$ sites that are close neighbors in the (111) plane ($V_{11}^{O^{(10)}-O^{(11)}}$) and in different (111) planes ($V_{11'}^{O^{(10)}-O^{(11)}}$) (Fig. 7c). Pair interactions between other $O^{(10)}$ and $O^{(11)}$ sites are deduced from symmetry (Fig. 7c). All other pair interactions are negligible and do not need to be considered in the Hamiltonian.

Using DFT, we compute the screw dislocation-hydrogen interaction energy (Eq. (2)) of thirty one configurations, which are described in supplementary materials. The ZPE contributions are neglected in these calculations. We then fit the eight different parameters of the Hamiltonian (four segregation energies and four pair interactions) on the obtained interaction energies using the least-squares method. The resulting set of parameters is presented in Table 5 and Fig. 8 shows a comparison of the energies calculated using the Ising model and from DFT. The energies predicted

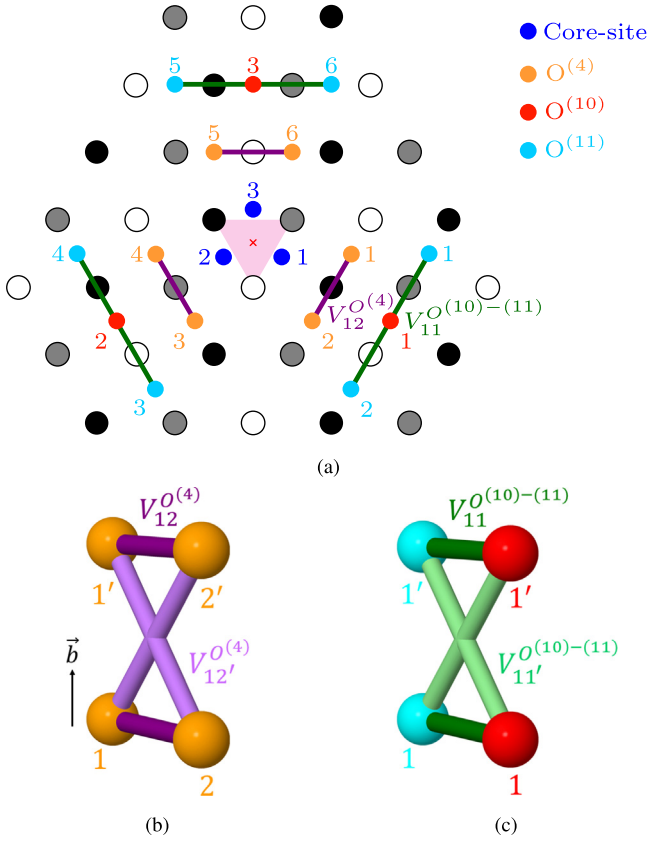

Fig. 7. Definition of the Ising model. Schematic representation of the considered sites and pair interactions (a) projected in the (111) plane and (b-c) along the Burgers vector direction for (b) $O^{(4)}$ sites and (c) $O^{(10)}$ and $O^{(11)}$ sites. The use of prime indicates a hydrogen atom belonging to a different (111) plane along the dislocation line.

Table 5
Energy parameters (eV) of the Ising model. The values including ZPE contributions are given in parentheses.

	W	Fe
$\Delta E^{seg,0}_{core}$	−0.66 (−0.75)	−0.15 (−0.22)
$\Delta E^{seg,0}_{O^{(4)}}$	−0.41 (−0.51)	−0.12 (−0.19)
$\Delta E^{seg,0}_{O^{(10)}}$	−0.27 (−0.35)	−0.08 (−0.17)
$\Delta E^{seg,0}_{O^{(11)}}$	−0.07 (−0.17)	0.00 (−0.07)
$V^{O^{(4)}}_{12}$	−0.46	−0.25
$V^{O^{(4)}}_{12'}$	0.41	0.24
$V^{O^{(10)-(11)}}_{11}$	−0.48	−0.17
$V^{O^{(10)-(11)}}_{11'}$	0.24	0.16

by the Ising model are very close to the DFT values (see also Table 1 in supplementary materials). We then include ZPE contributions in the segregation energies of the core-sites and the $O^{(4)}$, $O^{(10)}$ and $O^{(11)}$ sites. For the core-sites, we consider the ZPE contribution calculated in the case of the three core-sites occupied by hydrogen (Table 2), since we are interested in the temperature range in which core-sites remain fully saturated by hydrogen atoms. For the $O^{(4)}$, $O^{(10)}$ and $O^{(11)}$ sites, we consider the ZPE contributions calculated with one additional hydrogen inserted in one of these sites (Table 4).

Pair interactions of close O-sites (Table 5) are either highly attractive for hydrogen atoms in the same (111) plane ($V^{O^{(4)}}_{12}$ and $V^{O^{(10)-(11)}}_{11}$) or highly repulsive for hydrogen atoms in different (111) planes ($V^{O^{(4)}}_{12'}$ and $V^{O^{(10)-(11)}}_{11'}$). Part of this behavior can be attributed to Friedel oscillations. Indeed, the separation distance of hydrogen

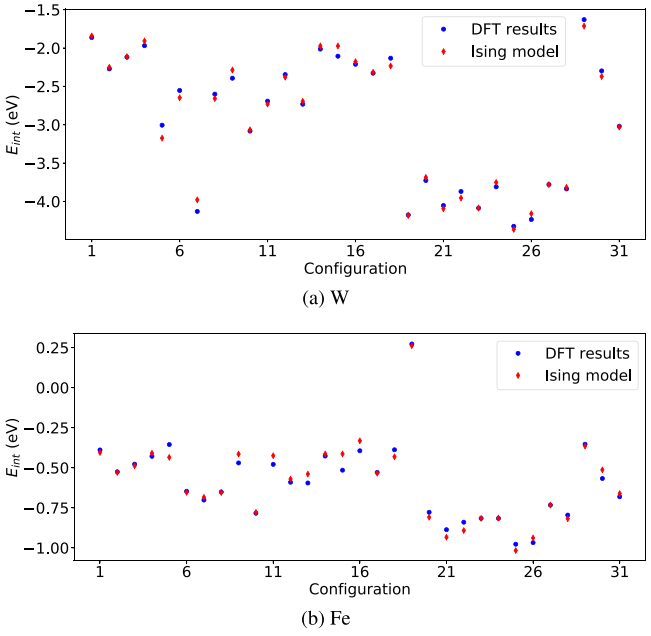

Fig. 8. Comparison between the interaction energies predicted by the Ising model (red diamonds) and obtained with DFT (blue circles) of the thirty one studied configurations. Interaction energies do not include ZPE contributions. A detailed description of the configurations as well as the values of the interactions energies and the relative errors are presented in supplementary materials. (For interpretation of the references to color in this figure legend, the reader is referred to the web version of this article.)

atoms is close to 0.90 a when they are in the same (111) plane and close to 1.15 a when they belong to different (111) planes, range in which Friedel oscillations are shown to be pronounced in bulk (§3.2). In the case of iron, considering the metal atom located between the hydrogen atoms in $O^{(4)}$ sites, we note either a weak decrease (0.18 μ_B/atom) or a weak increase (0.10 μ_B/atom) of the local atomic magnetic moment compared to the bulk value (2.19 μ_B/atom), when the hydrogen atoms are in the same (111) plane or in different (111) planes, respectively. We however reject the fact that the above mentioned behavior of the pair interactions between $O^{(4)}$ sites arises from magnetism, since we observe the same tendency in both tungsten and iron (Table 5).

5.2.2. Mean-field approximation

We consider the mean occupation [16,18,50] of the different attractive sites to express the equilibrium site concentrations of hydrogen as a function of temperature. We denote x_H^{core}, $x_H^{O^{(4)}}$, $x_H^{O^{(10)}}$ and $x_H^{O^{(10)}}$ the hydrogen concentration on core-sites, $O^{(4)}$, $O^{(10)}$ and $O^{(11)}$ sites, respectively. The mean-field Hamiltonian per unit of b is written as:

$$\langle H\rangle = 3\Delta E^{seg,0}_{core}x_H^{core} + 6\Delta E^{seg,0}_{O^{(4)}}x_H^{O^{(4)}} + 3\Delta E^{seg,0}_{O^{(10)}}x_H^{O^{(10)}} + 6\Delta E^{seg,0}_{O^{(11)}}x_H^{O^{(11)}} + 3\left(V^{O^{(4)}}_{12} + 2V^{O^{(4)}}_{12'}\right)\left(x_H^{O^{(4)}}\right)^2 + 6\left(V^{O^{(10)-(11)}}_{11} + 2V^{O^{(10)-(11)}}_{11'}\right)x_H^{O^{(10)}}x_H^{O^{(11)}}. \quad (9)$$

We then define $V^{O^{(4)}}_{OO} = V^{O^{(4)}}_{12} + 2V^{O^{(4)}}_{12'}$ and $V^{O^{(10)-(11)}}_{OO} = V^{O^{(10)-(11)}}_{11} + 2V^{O^{(10)-(11)}}_{11'}$, the average interaction between $O^{(4)}$ sites and between $O^{(10)}$ and $O^{(11)}$ sites, respectively. Considering the ideal configurational entropy, the free energy minimization leads to:

$$\frac{x_H^{core}}{1-x_H^{core}} = \frac{x_H^B}{1-x_H^B}\exp\left(-\frac{\Delta E^{seg,0}_{core}}{k_BT}\right). \quad (10)$$

$$\frac{x_H^{O^{(4)}}}{1-x_H^{O^{(4)}}} = \frac{x_H^B}{1-x_H^B}\exp\left(-\frac{\Delta E_{O^{(4)}}^{seg,0} + V_{OO}^{O^{(4)}} x_H^{O^{(4)}}}{k_B T}\right), \tag{11}$$

$$\frac{x_H^{O^{(10)}}}{1-x_H^{O^{(10)}}} = \frac{x_H^B}{1-x_H^B}\exp\left(-\frac{\Delta E_{O^{(10)}}^{seg,0} + 2V_{OO}^{O^{(10)-(11)}} x_H^{O^{(11)}}}{k_B T}\right), \tag{12}$$

$$\frac{x_H^{O^{(11)}}}{1-x_H^{O^{(11)}}} = \frac{x_H^B}{1-x_H^B}\exp\left(-\frac{\Delta E_{O^{(11)}}^{seg,0} + V_{OO}^{O^{(10)-(11)}} x_H^{O^{(10)}}}{k_B T}\right), \tag{13}$$

where k_B is the Boltzmann constant, T is the temperature and x_H^B is the hydrogen concentration in bulk. We then connect x_H^B to the nominal concentration of hydrogen atoms per metal atom, x_H^{nom}, through the conservation of hydrogen atoms in the system. In a given volume V, the number of T-sites in the bcc matrix is $N_B = 12V/a^3$, and the number of core-sites, $O^{(4)}$, $O^{(10)}$ and $O^{(11)}$ sites are respectively $N_{core} = 3\rho V/b$, $N_{O^{(4)}} = 2N_{core}$, $N_{O^{(10)}} = N_{core}$ and $N_{O^{(11)}} = 2N_{core}$, with ρ the dislocation density. Assuming that $N_B \gg N_{core} + N_{O^{(4)}} + N_{O^{(10)}} + N_{O^{(11)}}$ and given that six tetrahedral sites correspond to one metal atom, the matter conservation leads to:

$$\frac{x_H^{nom}}{6} = x_H^B + \frac{a^3\rho}{4b}\left(x_H^{core} + 2x_H^{O^{(4)}} + x_H^{O^{(10)}} + 2x_H^{O^{(11)}}\right). \tag{14}$$

We then use this relation to solve Eqs. (10)–(13) and obtain the temperature dependence of the hydrogen concentration on the different segregation sites for different nominal concentrations of hydrogen and different dislocation densities.

5.2.3. Segregation profiles

The segregation profiles, considering a typical dislocation density of 10^{12} m^{-2} and two different hydrogen nominal concentrations of 100 and 1000 appm, are shown in Fig. 9. Since the ZPE contributions to the segregation energies significantly increase the segregation energies (in absolute value) for all segregation sites (Table 5), the segregation profiles are shifted towards higher temperatures when we take into account these contributions. Core-sites remain fully decorated by hydrogen atoms at least up to 750 K in tungsten (Fig. 9a) and 200 K in iron (Fig. 9b). The increase of the nominal concentration results in an increase of this transition temperature from a fully saturated dislocation line ($x_H^{core} = 1$) to an almost empty line ($x_H^{core} = 0$). In order to provide a better comparison between both metals, Fig. 9 also presents the temperature range in terms of the homologous temperature defined as T/T_m, where T_m is the melting temperature ($T_m = 3695$ K for W and 1811 K for Fe [53]). Core-sites are shown to be completely decorated by hydrogen atoms in a homologous temperature range about two times larger in tungsten than in iron. This is due to the higher segregation energies compared to the melting temperature in tungsten than in iron. Our estimate of this transition temperature, 750 K in tungsten, is much higher than the value obtained by Wang et al. [19] (200 K) using a similar segregation model based on DFT calculations. The difference arises from the fact that Wang et al. considered the same interaction energy between H atoms in the core than in the bulk, while our calculations show that this interaction is negligible in the core, and thus differs from the strong repulsive interaction which exists in the bulk (Fig. 2). There is therefore no repulsion to prevent H clustering in the dislocation core, allowing for a full saturation of the core up to $\sim$ 750 K.

The octahedral sites $O^{(4)}$, $O^{(10)}$ and $O^{(11)}$ remain saturated with H atoms up to a lower transition temperature than core-sites. This is a consequence of the lower segregation energies for these octahedral sites, but also of the interaction which exists between these sites, in particular repulsive interactions. The same behavior is observed in tungsten and iron, with the $O^{(10)}$ sites being the last octahedral sites to remain fully saturated, before depletion of the core-sites, when the temperature increases. The main difference between both metals, in addition to the different temperature scale, is that the $O^{(11)}$ sites can be fully saturated in W at low temperature (below 250 K), while these sites remain almost completely depleted in Fe, because of the too small segregation energy (−0.07 eV with ZPE). As a consequence of the repulsive and attractive interactions between octahedral sites, some ordering may develop either in each atomic column of octahedral sites or between these columns. Such ordering tendency is not included in our simple mean-field approximation where the same homogeneous concentration is assumed in all columns of each different type. Ordering can be accounted for using either mean-field

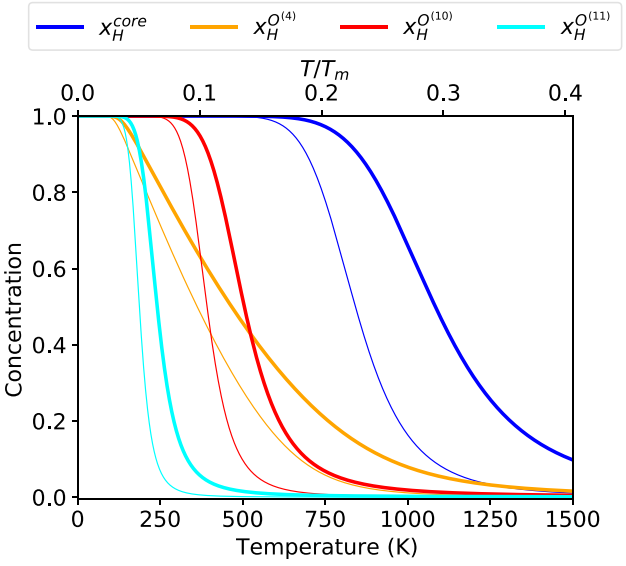

(a) W

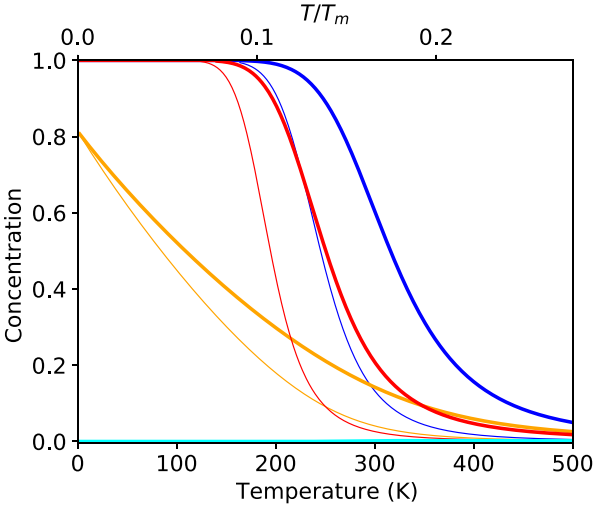

(b) Fe

Fig. 9. Temperature dependence of the hydrogen concentration segregated on the dislocation core-sites (blue), and on the $O^{(4)}$ (orange), $O^{(10)}$ (red) and $O^{(11)}$ (cyan) sites for nominal hydrogen concentrations of 1000 appm (thick lines) and 100 appm (thin lines) and for a dislocation density of 10^{12} m^{-2} in (a) W and (b) Fe. The upper x-axis indicates the homologous temperature defined as T/T_m, where T_m is the melting temperature. (For interpretation of the references to color in this figure legend, the reader is referred to the web version of this article.)

approximation with sublattices or kinetic Monte Carlo simulations [54]. Inclusions of these ordering tendencies will nevertheless not change the main result of the thermodynamic model, showing that the concentration of these octahedral sites falls down before the one of the core-sites.

The developed segregation model assumes that the dislocation core is in the hard core configuration. This assumption is valid only if hydrogen concentration is locally high enough to induce a reconstruction of the dislocation towards the hard core. *Ab initio* results discussed in section §4 indicate that the dislocation is pinned in the hard core configuration, or in a position close to this configuration, even when only one of the three core-sites is occupied by a hydrogen atom ($x_H^{core} = 1/3$), or when core-sites in only one in five (111) slabs are saturated with hydrogen ($x_H^{core} = 1/5$). One can therefore assume that the pinning of the dislocation by hydrogen atoms will remains efficient when the concentration of the core-sites is above 1/3, and probably still below this concentration. The thermodynamic model appears thus valid in the whole temperature range where the core-sites are saturated with H atoms, and still at the transition temperature where the concentration of these core-sites starts to fall down.

Finally, hydrogen segregation predicted from such a thermodynamic model will be possible only if hydrogen diffusion is fast enough to allow for thermal equilibrium, *i.e.* at not too low temperature. Considering the diffusion coefficient of hydrogen in tungsten [55] and iron [56], we can estimate the average time necessary for hydrogen to diffuse over the typical distance between dislocations, $1/\sqrt{\rho}$. For a dislocation density of $\rho = 10^{12}$ m^{-2}, this diffusion time becomes larger than one hour at 110 K and 50 K, in tungsten and iron respectively. Below these minimum temperatures, hydrogen atoms may not diffuse fast enough to reach equilibrium in a reasonable amount of time. Above, diffusion should not be a limiting factor anymore and one can expect that the dislocation cores are fully saturated by hydrogen atoms, as predicted by thermodynamics.

6. Conclusion

We demonstrate that the interaction between hydrogen and the dislocation core of the $1/2\langle 111\rangle$ screw dislocations is strongly attractive in both bcc tungsten and iron. Different core reconstructions are evidenced using DFT calculations, depending on the number of hydrogen atoms inside the core. The low energy state in both W and Fe corresponds to the hard core configuration with three hydrogen atoms per unit of b, lying in the face centers of the regular trigonal prisms constituting the hard core. As the occupation of the sites inside the core by hydrogen decreases along the dislocation line, this reconstructed core evolves towards a configuration in-between the hard and split cores in tungsten and it remains strongly pinned in the hard core configuration in iron, up to an occupation of 1/5. ZPE contributions, arising from H vibrations, are significant and reinforce the attraction between the dislocation core and the hydrogen atoms, particularly in iron.

Hydrogen attraction is not limited to the core-sites inside the reconstructed dislocation and other sites, around the reconstructed line, are attractive in both W and Fe. Indeed, according to our DFT calculations, the fourth, tenth and eleventh neighbor octahedral sites of the reconstructed core are attractive, with an interaction energy similar to that of the core-sites. The other tetrahedral and octahedral sites around the reconstructed core are either repulsive or unstable for hydrogen. At a distance of 2.4 lattice parameters from the core, namely beyond the eighteenth neighbor octahedral sites of the core, the interaction energy falls very close to zero and the hydrogen atom recovers its behavior in the perfect bcc lattice, where the octahedral sites are unstable and the tetrahedral sites are stable.

On the basis of our DFT results, we develop an Ising model in W and Fe, taking into account both the core-sites and the three attractive octahedral sites around the reconstructed core. Using mean-field calculations, we express the hydrogen equilibrium concentrations on the different sites as a function of temperature. The segregation profiles show that the core-sites remain fully saturated by hydrogen atoms with the dislocation adopting a hard core configuration up to room temperature in iron and a higher temperature (about 750 K) in tungsten, in agreement with the highest melting temperature and the strongest hydrogen binding in tungsten.

The hydrogen segregation on screw dislocation cores in tungsten and iron is similar to the segregation already evidenced in these metals with carbon addition, where the dislocation also adopts a hard core configuration [18,50]. The dislocation core reconstruction induced by hydrogen segregation is however more complex as three different attractive sites per unit of Burgers vector are found for hydrogen in the dislocation core, instead of one unique attractive site for carbon. As already demonstrated with carbon in both Fe [57–59] and W [60], this hydrogen segregation on screw dislocations is expected to have a strong impact on their glide motion. In particular, it should probably be necessary to consider that screw dislocations are gliding at low temperatures with their solute atmosphere, to understand the enhancement of screw dislocations mobility, which is seen experimentally [3,5].

Declaration of Competing Interest

The authors declare that they have no known competing financial interests or personal relationships that could have appeared to influence the work reported in this paper.

Acknowledgments

The authors acknowledge support from the Agence Nationale de la Recherche through the DeGAS project (ANR-16-CE08-0008). The authors also acknowledge Partnership for Advanced Computing in Europe for funding DIMAB project by providing computing time on the Juwels supercomputer at Jülich Supercomputing Centre. This work has been carried out within the framework of the EUROfusion Consortium, funded by the European Union via the Euratom Research and Training Programme (Grant Agreement No 101052200–EUROfusion). Views and opinions expressed are however those of the author(s) only and do not necessarily reflect those of the European Union or the European Commission. Neither the European Union nor the European Commission can be held responsible for them.

Supplementary material

Supplementary material associated with this article can be found, in the online version, at10.1016/j.actamat.2022.118048.

References

[1] M.L. Martin, M. Dadfarnia, A. Nagao, S. Wang, P. Sofronis, Enumeration of the hydrogen-enhanced localized plasticity mechanism for hydrogen embrittlement in structural materials, Acta Mater. 165 (2019) 734–750, doi:10.1016/j.actamat.2018.12.014.
[2] I.M. Robertson, P. Sofronis, A. Nagao, M.L. Martin, S. Wang, D.W. Gross, K.E. Nygren, Hydrogen embrittlement understood, Metall. Mater. Trans. B 46 (3) (2015) 1085–1103, doi:10.1007/s11663-015-0325-y.
[3] T. Tabata, H.K. Birnbaum, Direct observations of the effect of hydrogen on the behavior of dislocations in iron, Scr. Metall. 17 (1983) 947–950, doi:10.1016/0036-9748(83)90268-5.
[4] J. Song, W.A. Curtin, Atomic mechanism and prediction of hydrogen embrittlement in iron, Nat. Mater. 12 (2013) 145–151, doi:10.1038/nmat3479.
[5] L.-C. Huang, D. Chen, D.-G. Xie, S. Li, T. Zhu, D. Raabe, E. Ma, J. Li, Z.-W. Shan, Quantitative tests revealing hydrogen enhanced dislocation motion in α-iron, 2021, doi:10.21203/rs.3.rs-1059604/v1.

[6] J.P. Hirth, J. Lothe, Theory of Dislocations, second ed., Wiley, New York, 1982.
[7] D. Caillard, J. Martin, Thermally Activated Mechanisms of Crystal Plasticity, Pergramon, Amsterdam, 2003.
[8] L. Romaner, C. Ambrosch-Draxl, R. Pippan, Effect of rhenium on the dislocation core structure in tungsten, Phys. Rev. Lett. 104 (2010) 195503, doi:10.1103/PhysRevLett.104.195503.
[9] H. Li, S. Wurster, C. Motz, L. Romaner, C. Ambrosch-Draxl, R. Pippan, Dislocation-core symmetry and slip planes in tungsten alloys: *ab initio* calculations and microcantilever bending experiments, Acta Mater. 60 (2012) 748–758, doi:10.1016/j.actamat.2011.10.031.
[10] D.R. Trinkle, C. Woodward, The chemistry of deformation: how solutes soften pure metals, Science 310 (5754) (2005) 1665–1667, doi:10.1126/science.1118616.
[11] Y.J. Hu, M.R. Fellinger, B.G. Bulter, Y. Wang, K.A. Darling, L.J. Kecskes, D.R. Trinkle, Z.K. Liu, Solute-induced solid-solution softening and hardening in BCC tungsten, Acta Mater. 141 (2017) 304–316, doi:10.1016/j.actamat.2017.09.019.
[12] T. Tsuru, T. Suzudo, First-principles calculations of interaction between solutes and dislocations in tungsten, Nucl. Mater. Energy 16 (2018) 221–225, doi:10.1016/j.nme.2018.07.007.
[13] Y. Zhao, L. Dezerald, M. Pozuelo, X. Zhou, J. Marian, Simulating the mechanisms of serrated flow in interstitial alloys with atomic resolution over diffusive timescales, Nat. Commun. 11 (2020) 1227, doi:10.1038/s41467-020-15085-3.
[14] B. Lüthi, L. Ventelon, C. Elssser, D. Rodney, F. Willaime, First principles investigation of carbon-screw dislocation interactions in body-centered cubic metals, Modelling Simul. Mater. Sci. Eng. 25 (8) (2017) 084001, doi:10.1088/1361-651x/aa88eb.
[15] A. Bakaev, A. Zinovev, D. Terentyev, G. Bonny, C. Yin, N. Castin, Y.A. Mastrikov, E.E. Zhurkin, Interaction of carbon with microstructural defects in a W-Re matrix: An *ab initio* assessment, J. Appl. Phys. 126 (7) (2019) 075110, doi:10.1063/1.5094441.
[16] L. Ventelon, B. Lüthi, E. Clouet, L. Proville, B. Legrand, D. Rodney, F. Willaime, Dislocation core reconstruction induced by carbon segregation in BCC iron, Phys. Rev. B 91 (22) (2015) 1–5, doi:10.1103/PhysRevB.91.220102.
[17] B. Lüthi, L. Ventelon, D. Rodney, F. Willaime, Attractive interaction between interstitial solutes and screw dislocations in BCC iron from first principles, Comput. Mater. Sci. 148 (2018) 21–26, doi:10.1016/j.commatsci.2018.02.016.
[18] G. Hachet, L. Ventelon, F. Willaime, E. Clouet, Screw dislocation-carbon interaction in BCC tungsten: an *ab initio* study, Acta Mater. 200 (2020) 481–489, doi:10.1016/j.actamat.2020.09.014.
[19] Y. Wang, X. Wang, X. Wu, Q. Li, C. Li, G. Shu, B. Xu, W. Liu, Hydrogen distribution induced screw dislocation core spreading in tungsten, J. Nucl. Mater. 523 (2019) 71–79, doi:10.1016/j.jnucmat.2019.05.038.
[20] A. Bakaev, P. Grigorev, D. Terentyev, A. Bakaeva, E.E. Zhurkin, Y.A. Mastrikov, Trapping of hydrogen and helium at dislocations in tungsten: an *ab initio* study, Nucl. Fusion 57 (12) (2017) 126040, doi:10.1088/1741-4326/aa7965.
[21] P. Grigorev, T.D. Swinburne, J.R. Kermode, Hybrid quantum/classical study of hydrogen-decorated screw dislocations in tungsten: ultrafast pipe diffusion, core reconstruction, and effects on glide mechanism, Phys. Rev. Mater. 4 (2) (2020) 023601, doi:10.1103/PhysRevMaterials.4.023601.
[22] M. Itakura, H. Kaburaki, M. Yamaguchi, T. Okita, The effect of hydrogen atoms on the screw dislocation mobility in bcc iron: a first-principles study, Acta Mater. 61 (2013) 6857–6867, doi:10.1016/j.actamat.2013.07.064.
[23] Y. Zhao, G. Lu, QM/MM study of dislocation—hydrogen/helium interactions in α-Fe, Modelling Simul. Mater. Sci. Eng. 19 (6) (2011) 065004, doi:10.1088/0965-0393/19/6/065004.
[24] I.H. Katzarov, D.L. Pashov, A.T. Paxton, Hydrogen embrittlement I. Analysis of hydrogen-enhanced localized plasticity: effect of hydrogen on the velocity of screw dislocations in α-Fe, Phys. Rev. Mater. 1 (2017) 033602, doi:10.1103/PhysRevMaterials.1.033602.
[25] P. Hohenberg, W. Kohn, Inhomogeneous electron gas, Phys. Rev. 136 (3B) (1964) B864–B871, doi:10.1103/PhysRev.136.B864.
[26] W. Kohn, L.J. Sham, Self-consistent equations including exchange and correlation effects, Phys. Rev. 140 (4) (1965) A1133–A1138, doi:10.1103/PhysRev.140.A1133.
[27] G. Kresse, J. Furthmüller, Efficient iterative schemes for *ab initio*total-energy calculations using a plane-wave basis set, Phys. Rev. B 54 (16) (1996) 11169–11186, doi:10.1103/PhysRevB.54.11169.
[28] P.E. Blöchl, Projector augmented-wave method, Phys. Rev. B 50 (24) (1994) 17953, doi:10.1103/PhysRevB.50.17953.
[29] G. Kresse, D. Joubert, From ultrasoft pseudopotentials to the projector augmented-wave method, Phys. Rev. B 59 (3) (1999) 1758–1775, doi:10.1103/PhysRevB.59.1758.
[30] J. Perdew, K. Burke, M. Ernzerhof, Generalized gradient approximation made simple, Phys. Rev. Lett. 77 (18) (1996) 3865–3868, doi:10.1103/PhysRevLett.77.3865.
[31] M. Methfessel, A.T. Paxton, High-precision sampling for Brillouin-zone integration in metals, Phys. Rev. B 40 (1989) 3616–3621, doi:10.1103/PhysRevB.40.3616.
[32] G. Henkelman, B.P. Uberuaga, H. Jónsson, A climbing image nudged elastic band method for finding saddle points and minimum energy paths, J. Chem. Phys. 113 (22) (2000) 9901–9904, doi:10.1063/1.1329672.
[33] G. Henkelman, H. Jónsson, Improved tangent estimate in the nudged elastic band method for finding minimum energy paths and saddle points, J. Chem. Phys. 113 (22) (2000) 9978–9985, doi:10.1063/1.1323224.
[34] E. Hayward, C.-C. Fu, Interplay between hydrogen and vacancies in α-Fe, Phys. Rev. B 87 (2013) 174103, doi:10.1103/PhysRevB.87.174103.
[35] W.A. Counts, C. Wolverton, R. Gibala, First-principles energetics of hydrogen traps in α-Fe: point defects, Acta Mater. 58 (14) (2010) 4730–4741, doi:10.1016/j.actamat.2010.05.010.
[36] D. Rodney, L. Ventelon, E. Clouet, L. Pizzagalli, F. Willaime, *Ab initio* modeling of dislocation core properties in metals and semiconductors, Acta Mater. 124 (2017) 633–659, doi:10.1016/j.actamat.2016.09.049.
[37] E. Clouet, *Ab initio* models of dislocations, in: W. Andreoni, S. Yip (Eds.), Handbook of Materials Modeling, Springer International Publishing, 2018, pp. 1–22, doi:10.1007/978-3-319-42913-7_22-1.
[38] E. Clouet, L. Ventelon, F. Willaime, Dislocation core energies and core fields from first principles, Phys. Rev. Lett. 102 (5) (2009) 1–4, doi:10.1103/PhysRevLett.102.055502.
[39] L. Ventelon, F. Willaime, E. Clouet, D. Rodney, *Ab initio* investigation of the Peierls potential of screw dislocations in bcc Fe and W, Acta Mater. 61 (11) (2013) 3973–3985, doi:10.1016/j.actamat.2013.03.012.
[40] L. Dezerald, L. Ventelon, E. Clouet, C. Denoual, D. Rodney, F. Willaime, *Ab initio* modeling of the two-dimensional energy landscape of screw dislocations in BCC transition metals, Phys. Rev. B 89 (024104) (2014) 1–13, doi:10.1103/PhysRevB.89.024104.
[41] N. Fernandez, Y. Ferro, D. Kato, Hydrogen diffusion and vacancies formation in tungsten: density functional theory calculations and statistical models, Acta Mater. 94 (2015) 307–318, doi:10.1016/j.actamat.2015.04.052.
[42] Y.-L. Liu, Y. Zhang, G.-N. Luo, G.-H. Lu, Structure, stability and diffusion of hydrogen in tungsten: a first-principles study, J. Nucl. Mater. 390-391 (2009) 1032–1034, doi:10.1016/j.jnucmat.2009.01.277.
[43] A.S. Kholtobina, R. Pippan, L. Romaner, D. Scheiber, W. Ecker, V.I. Razumovskiy, Hydrogen trapping in bcc Iron, Materials 13 (10) (2020), doi:10.3390/ma13102288.
[44] D.E. Jiang, E.A. Carter, Diffusion of interstitial hydrogen into and through bcc Fe from first principles, Phys. Rev. B 70 (2004) 064102, doi:10.1103/PhysRevB.70.064102.
[45] R. Frauenfelder, Solution and diffusion of hydrogen in tungsten, J. Vac. Sci. Technol. 6 (1969) 388, doi:10.1116/1.1492699.
[46] J.P. Hirth, Effects of hydrogen on the properties of iron and steel, Metall. Mater. Trans. A 11 (6) (1980) 861–890, doi:10.1007/bf02654700.
[47] K. Christmann, Interaction of hydrogen with solid surfaces, Surf. Sci. Rep. 9 (1) (1988) 1–163, doi:10.1016/0167-5729(88)90009-X.
[48] K. Heinola, T. Ahlgren, Diffusion of hydrogen in bcc tungsten studied with first principle calculations, J. Appl. Phys. 107 (11) (2010) 113531, doi:10.1063/1.3386515.
[49] C.S. Becquart, C. Domain, A density functional theory assessment of the clustering behaviour of He and H in tungsten, J. Nucl. Mater. 386-388 (2009) 109–111, doi:10.1016/j.jnucmat.2008.12.085.
[50] B. Lüthi, F. Berthier, L. Ventelon, B. Legrand, D. Rodney, F. Willaime, *Ab initio* thermodynamics of carbon segregation on dislocation cores in BCC iron, Modelling Simul. Mater. Sci. Eng. 27 (7) (2019) 074002, doi:10.1088/1361-651X/ab28d4.
[51] J.M. Sanchez, F. Ducastelle, D. Gratias, Generalized cluster description of multicomponent systems, Physica A 128 (1984) 334–350, doi:10.1016/0378-4371(84)90096-7.
[52] L. Casillas-Trujillo, B. Alling, Configurational thermodynamics of a $1/2\langle 111\rangle$ screw dislocation core in Mo–W solid solutions using cluster expansion, J. Appl. Phys. 128 (2020) 045114, doi:10.1063/5.0011379.
[53] W.M. Haynes, CRC Handbook of Chemistry and Physics, 92 ed., CRC Press, Boca Raton, 2011.
[54] F. Berthier, 2021, Private communication.
[55] D.F. Johnson, E.A. Carter, Hydrogen in tungsten: absorption, diffusion, vacancy trapping, and decohesion, J. Mater. Res. 25 (2) (2010) 315–327, doi:10.1557/JMR.2010.0036.
[56] H. Hagi, Diffusion coefficient of hydrogen in iron without trapping by dislocations and impurities, Mater. Trans. 35 (2) (1994) 112–117, doi:10.2320/matertrans1989.35.112.
[57] D. Caillard, J. Bonneville, Dynamic strain aging caused by a new Peierls mechanism at high-temperature in iron, Scr. Mater. 95 (1) (2015) 15–18, doi:10.1016/j.scriptamat.2014.09.019.
[58] D. Caillard, Dynamic strain ageing in iron alloys: the shielding effect of carbon, Acta Mater. 112 (2016) 273–284, doi:10.1016/j.actamat.2016.04.018.
[59] B. Lüthi, Modélisation ab initio des interactions entre dislocations vis et solutés interstitiels dans les métaux de transition cubiques centrés, Univ. Lyon, France, 2017 Ph.D. thesis. https://tel.archives-ouvertes.fr/tel-01630129/
[60] G. Hachet, D. Caillard, L. Ventelon, E. Clouet, Mobility of screw dislocation in BCC tungsten at high temperature in presence of carbon, Acta Mater. 222 (2022) 117440, doi:10.1016/j.actamat.2021.117440.